Asian Journal of Chemistry; Vol. 30, No. 2 (2018), 343-350

ASIAN JOURNAL OF CHEMISTRY

https://doi.org/10.14233/ajchem.2018.20957

Growth, Spectral, Thermal, Linear and Non-Linear Optical Characteristics of an Efficient Organic Crystal: L-Lysinium 5-Sulfosalicylate

R. USHA, N. HEMA, V. REVATHI AMBIKA, D. SHALINI and D. JAYALAKSHMI*

PG & Research Department of Physics, Queen Mary's College, Chennai-600 004, India

*Corresponding author: E-mail: djayalakshmi2016@gmail.com

Received: 7 August 2017; *Accepted*: 9 November 2017; *Published online*: 31 December 2017; AJC-18703

L-Lysinium 5-sulfosalicylate (LL5SS) has been synthesized and grown by solution growth method at room temperature using deionized water as a solvent. The crystal structure of the materials was solved by single crystal X-ray diffraction analysis and it was found that the material has monoclinic system with the space group $P2_1$. Fourier transform infrared spectral study was carried out to confirm functional groups present in the crystal. The optical absorption study shows that the crystal is transparent in the entire visible region with a cut-off wavelength of 324 nm. Photoluminescence studies were also carried out to identify the excitation emission of the grown LL5SS crystal. Dielectric study was performed on the single crystal to study the power dissipation of the material in the presence of alternating electric field. Thermal stability has been assessed by thermo gravimetric analysis. Mechanical parameters were calculated. The laser damage threshold value of LL5SS crystal was estimated to be 5.6 GW/cm^2 using a Nd:YAG laser. The Kurtz and Perry powder SHG efficiencies were measured. Non-linear refractive index (n_2), non-linear absorption coefficient (β) and third-order non-linear optical susceptibility (χ^3) values of LL5SS were found from Z scan technique.

Keywords: Single crystal XRD, Photoluminesence, Dielectric measurement, Third order non-linear optical property, Micro hardness.

INTRODUCTION

Nowadays, much consideration was provided to the non-linear optical materials, which are the main focus of many research works going on around the world. The role of organic non-linear optical (NLO) materials with large optical non-linearity in the fabrication of devices in telecommunication, optical information processing and high optical disk data storage is immensely significant [1-7]. Organic materials are the prime choice of researchers because they have tendency to show higher order of non-linearity. The laser beam interacts with the delocalized π-electrons existing in the organic molecule produce non-linear polarization. The non-linear susceptibility of an organic material would be larger when it has donor–acceptor conjugated molecular systems. Normally amino acids have the tendency to crystallize in a non-centrosymmetric form which is useful for non-linear optical applications. A sequence of second order/third order NLO active materials composed of L-Lysine have been synthesized, such as, L-lysinium picrate, L-Lysine adipate, L-lysine acetate, tetra L-Lysine alanine mono hydrochloride dehydrate [8-11]. From the coordination chemistry, 5-sulfosalicylicacid (5SSA) is especially an attractive ligand, possessing three potential coordination groups such as OH, COOH and SO_3H [12-15].

In this work, the single crystal of L-lysinium 5-sulfosalicylate (LL5SS), an organic NLO compound has been synthesized by slow evaporation method in aqueous solution at room temperature. In this work, the structural, optical, dielectric, hardness, photoluminescence, laser threshold damage, second and third order non linearity characterization of LL5SS are reported.

EXPERIMENTAL

Synthesis: The high purity L-Lysine monohydrochloride was mixed with 5-sulfosalicylic acid in the molar ratio of 1:1 and it was dissolved in deionized water. The chemical reaction scheme is given in Fig. 1. The solution was stirred well using magnetic stirrer for about 5 h at 40 °C and it was filtered using Whatman filter paper and kept for evaporation in a constant temperature bath (CTB). The purity of the LL5SS salt was enhanced by recrystalizing the salt four times. Colourless needle shaped crystals of LL5SS having a typical size of 12 mm × 5 mm × 2 mm were collected in 20 days and the photograph of grown crystal is presented in Fig. 2.

Solubility: Solubility of a material in a particular solvent defines the super saturation which is the driving force for the rate of crystal growth. The solubility data were determined by

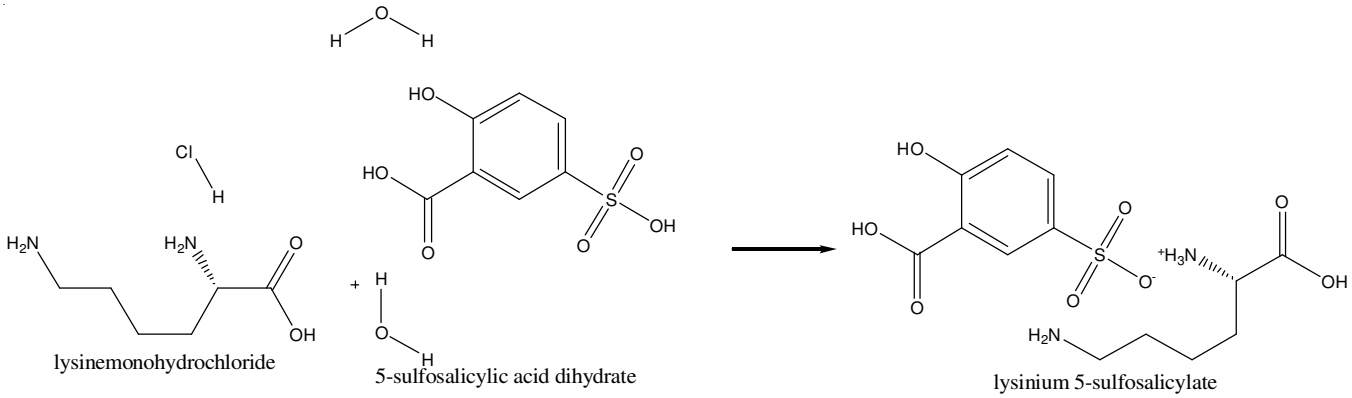

Fig. 1. Reaction scheme of LL5SS material

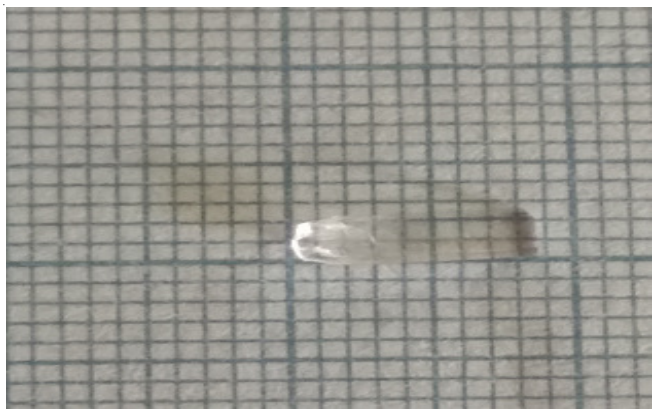

Fig. 2. As-grown crystal of LL5SS

dissolving the synthesized salt of LL5SS in 100 mL solvent at a constant temperature with continuous stirring. After attaining saturation, the equilibrium concentration of the solute was analyzed gravimetrically. The solubility of LL5SS has been determined for different temperatures, 30, 40 and 50 °C, respectively as shown in Fig. 3.

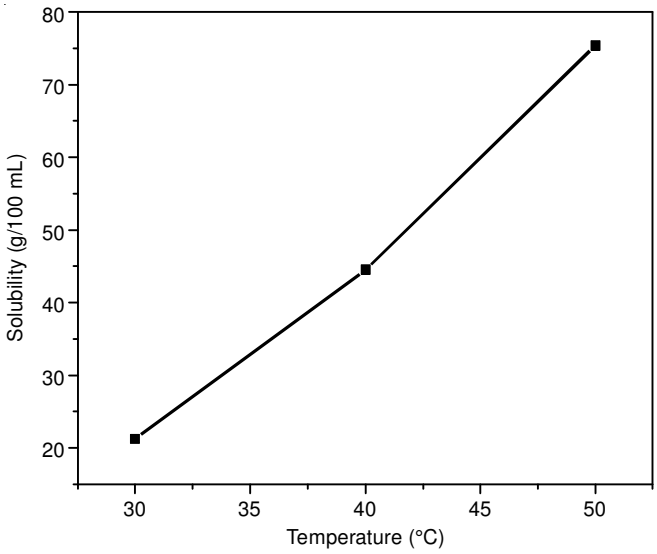

Fig. 3. Solubility curve of LL5SS in water

RESULTS AND DISCUSSION

Single crystal X-ray diffraction studies: The single crystal X-ray diffraction studies have been carried out to confirm the crystallinity and to determine the lattice parameters of the grown sample. The single crystal of LL5SS with dimensions 0.250 mm × 0.220 mm × 0.120 mm was chosen for X-ray diffraction study. The structure of LL5SS was solved by the direct method using SHELXL-2014/7 fined by the full-matrix least squares methods on F^2. A Bruker kappa APEXII single crystal X-ray Diffractometer with MoK_α (λ = 0.71073 Å) radiation was used for X-ray diffraction study. The calculated lattice parameter values are a = 6.8770 Å, b = 16.4266 Å, c = 11.9729 Å and V = 1351.39 A^3. LL5SS crystallizes in monoclinic system with noncentro symmetric space group $P2_1$. The crystal data and the structure refinement for LL5SS material is given in Table-1. The ORTEP diagram of the grown LL5SS single crystal is shown in Fig. 4. The structure was solved using collected/unique reflections 10406/4681 [R(int) = 0.0177]. The

TABLE-1
CRYSTAL DATA AND STRUCTURE REFINEMENT FOR LL5SS

Identification code	L5SS
Empirical formula	$C_{20}H_{30}N_2O_{17}S_2$
Formula weight	634.58
Temperature	296(2) K
Wavelength	0.71073 A
Crystal system, space group	Monoclinic, $P2_1$
Unit cell dimensions	a = 6.8770(2) Å α = 90° b = 16.4266(4) Å;β = 92.3535(14)° c = 11.9729(3) Å; γ = 90°
Volume	1351.39(6) $Å^3$
Z, Calculated density	2, 1.559 Mg/m^3
Absorption coefficient	0.282 mm^{-1}
F(000)	664
Crystal size	0.250 × 0.220 × 0.120 mm
Theta range for data collection	1.702 to 25.000°
Limiting indices	-7 <= h <= 8, -19 <= k <= 19, -14 <= l <= 14
Reflections collected/unique	10406/4681 [R(int) = 0.0177]
Completeness to theta = 25.000°	100.0 %
Absorption correction	None
Refinement method	Full-matrix least-squares on F^2
Data/restraints/parameters	4681/2/427
Goodness-of-fit on F^2	1.070
Final R indices [I>2σ(I)]	R1 = 0.0270, wR2 = 0.0679
R indices (all data)	R1 = 0.0284, wR2 = 0.0688
Absolute structure parameter	0.006(18)
Extinction coefficient	n/a
Largest diff. peak and hole	0.273 and -0.365 $e.A^{-3}$
CCDC	1562492

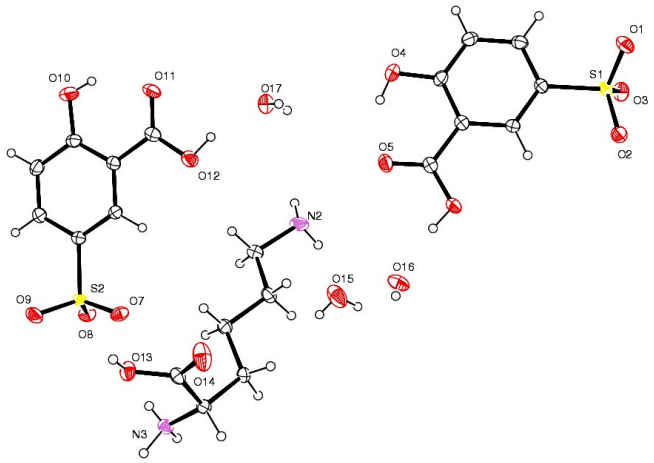

Fig. 4. ORTEP diagram of LL5SS

goodness-of-fit was 1.066. The crystallographic data (CIF) for the molecule compound structure reported in this paper have been deposited in the Cambridge Crystallographic Data Centre as supplementary material number CCDC 1562492.The bond length is given in Table-2. Hydrogen bond distances and angles given in Table-3.

Fourier transform infrared spectroscopy analysis: FTIR spectroscopy is an important tool to identify the presence of various functional group and the types of vibration in the material. FTIR transmission spectrum of LL5SS crystal was recorded in the region 4000-400 cm^{-1} employing a Perkin Elmer spectrometer by KBr pellet method is shown in Fig. 5. The frequency assignment for LL5SS with various functional groups is presented in Table-4. The peak observed at 3522 cm^{-1} is assigned to NH stretching vibration. The broad peak at 3094 cm^{-1} is due to the presence of water molecule in the crystal. The vibrational band at 1741 cm^{-1} is due to the C=O stretching vibration. The asymmetric and symmetric bending vibrations are observed at 1611 and 1517 cm^{-1}. The peaks at 1497 cm^{-1} and 1474 cm^{-1} are attributed to CH scissoring and wagging. The bending vibrations of OH group are observed at 1440 cm^{-1}. The peaks at about 1328 and 1024 cm^{-1} assigned for CN stretching vibrations. The CO stretching vibration band appeared at 1290 cm^{-1}. The peak with wave number at 1161 cm^{-1} was observed for the rocking NH_3 structure. The band at 910 cm^{-1} is due to the CC stretching vibration. The sharp peak at 841 cm^{-1} is due to the out of plane bending vibration of hydrogen bonds. The CH bending vibration and CS stretching vibrations absorbed at 819 and 793 cm^{-1}. The COO^- scissoring, SO_2 scissoring, SO_2 wagging vibrations are positioned at 711, 588, 529 cm^{-1} respectively. This observation confirms the formation of LL5SS compound.

UV-visible spectroscopy: The optical property of the LL5SS compound has been assessed by using LAMBDA-35 UV spectrometer in the wavelength range of 200-800 nm. The UV-visible studies give structural information. Absorption of UV and visible light involves promotion of the electrons in π and σ orbitals from the ground state to higher energy states. Lower UV cut off wavelength plays an important role in identifying

TABLE-2
BOND LENGTHS (Å) FOR LL5SS

C1-C6	1.375(4)	C1-C2	1.392(4)
C1-S1	1.772(3)	C2-C3	1.381(4)
C2-H2	0.93	C3-C4	1.386(5)
C3-H3	0.93	C4-O4	1.352(4)
C4-C5	1.409(4)	C5-C6	1.403(4)
C5-C7	1.475(4)	C6-H6	0.93
C7-O5	1.224(4)	C7-O6	1.312(4)
C8-C9	1.371(4)	C8-C13	1.397(4)
C8-S2	1.765(3)	C9-C10	1.399(4)
C9-H9	0.93	C10-C11	1.395(4)
C10-C14	1.471(4)	C11-O10	1.349(4)
C11-C12	1.398(5)	C12-C13	1.376(4)
C12-H12	0.93	C13-H13	0.93
C14-O11	1.220(4)	C14-O12	1.323(4)
C15-N2	1.491(4)	C15-C16	1.505(4)
C15-H15A	0.97	C15-H15B	0.97
C16-C17	1.528(4)	C16-H16A	0.97
C16-H16B	0.97	C17-C18	1.525(4)
C17-H17A	0.97	C17-H17B	0.97
C18-C19	1.521(4)	C18-H18A	0.97
C18-H18B	0.97	C19-N3	1.476(4)
C19-C20	1.520(4)	C19-H19	0.98
C20-O14	1.200(4)	C20-O13	1.308(4)
N2-H4N	1.00(4)	N2-H5N	0.90(4)
N2-H6N	0.84(5)	N3-H2N	0.93(4)
N3-H1N	0.74(4)	N3-H3N	0.98(4)
O1-S1	1.451(2)	O2-S1	1.461(2)
O3-S1	1.454(2)	O4-H8O	0.86(5)
O6-H1O	0.89(4)	O7-S2	1.468(2)
O8-S2	1.449(2)	O9-S2	1.448(2)
O10-H10	0.82	O12-H2O	0.90(3)
O13-H5O	0.73(4)	O15-H4O	0.82(5)
O15-H3O	0.77(6)	O16-H9O	0.62(3)
O17-H7O	0.87(4)	O17-H6O	0.75(4)

TABLE-3
HYDROGEN BOND DISTANCES (Å) AND ANGLES (°) FOR LL5SS

	Donor-H	Acceptor-H	Donor-Acceptor	Angle
N2-H6N···O9	0.84(5)	2.23(5)	2.895(4)	136.(4)
N2-6N···O5	0.84(5)	2.45(5)	2.958(4)	120.(4)
O4-8O···O5	0.86(5)	1.83(5)	2.604(4)	150.(4)
O12H2O···O17	0.90(3)	1.84(3)	2.704(3)	160.(6)
O6-H1O···O16	0.89(4)	1.71(4)	2.588(3)	168.(3)
O16-H9O···O2	0.62(3)	2.19(4)	2.810(4)	173.(4)
N2-H5N···O8	0.90(4)	2.13(4)	2.961(4)	154.(3)
N2-H4N···O15	1.00(4)	1.83(4)	2.790(4)	162.(4)
N3-H3N···O11	0.98(4)	2.20(4)	2.848(4)	122.(3)
N3-H3N···O3	0.98(4)	2.01(4)	2.853(4)	143.(3)
N3-H1N···O17	0.74(4)	2.20(4)	2.905(4)	162.(4)
N3-H2N···O1	0.93(4)	1.91(4)	2.791(4)	157.(3)
O17-H6O···O8	0.75(4)	2.19(4)	2.859(3)	148.(4)
O17-H7O···S2	0.87(4)	2.82(4)	3.667(3)	162.(4)
O17-H7O···O9	0.87(4)	2.67(4)	3.321(4)	133.(4)
O17-H7O···O7	0.87(4)	2.04(4)	2.887(3)	164.(4)
O13-H5O···S2	0.73(4)	2.89(4)	3.427(2)	132.(3)
O13-H5O···O7	0.73(4)	1.95(4)	2.652(3)	159.(4)
O15-H3O···O14	0.77(6)	2.14(6)	2.865(4)	158.(6)
O15-H4O···S1	0.82(5)	2.81(5)	3.570(3)	154.(4)
O15-H4O···O3	0.82(5)	2.63(5)	3.157(4)	124.(4)
O15-H4O···O2	0.82(5)	2.05(5)	2.870(4)	175.(4)
O10-H10···O11	0.82	1.89	2.598(3)	144.5
C19-H19···O6	0.98	2.59	3.330(3)	132.5
C15-H15A···O14	0.97	2.61	3.315(4)	129.4
C2- H2···O13	0.93	2.6	3.480(4)	158.6

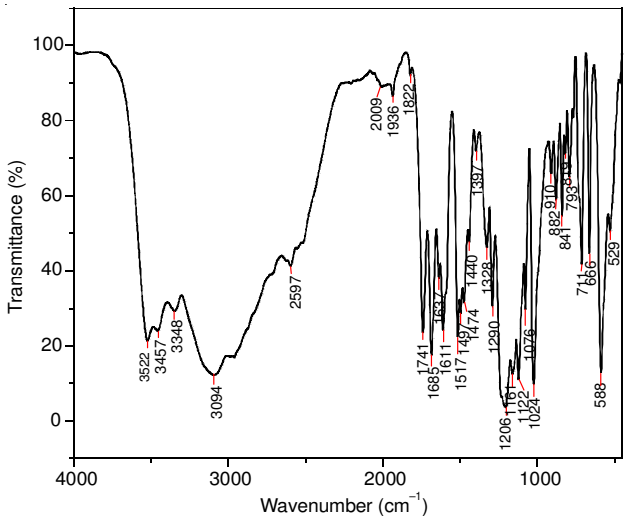

Fig. 5. FTIR spectrum of LL5SS

TABLE-4
FT-IR ASSIGNMENTS OF LL5SS

Wavenumber (cm^{-1})	Assignments
3522	NH_3^+ symmetric stretching
3094	OH stretching vibration
1685	C=O stretching frequency of COOH
1611	NH_3^+Asymmetric bending vibration
1517	NH_3^+ Symmetric bending vibration
1290	C-O Stretching vibration
1161	Rocking of NH_3^+
910	C-C Stretching vibration
711	COO^- scissoring
588	SO_2 scissoring
529	SO_2 Wagging

the potential of an NLO material. The lower cut off wavelength of the crystal is found to be 324 nm and there is no absorption of light to any appreciable extent in the visible range of the electromagnetic spectrum [16]. The optical band gap of LL5SS crystal was determined using Tauc's extrapolation method as depicted in Fig. 6. The optical band gap of LL5SS is found to be 3.536 eV. The large value of band gap indicates that the crystal can be suitable material for the optoelectronics and NLO applications.

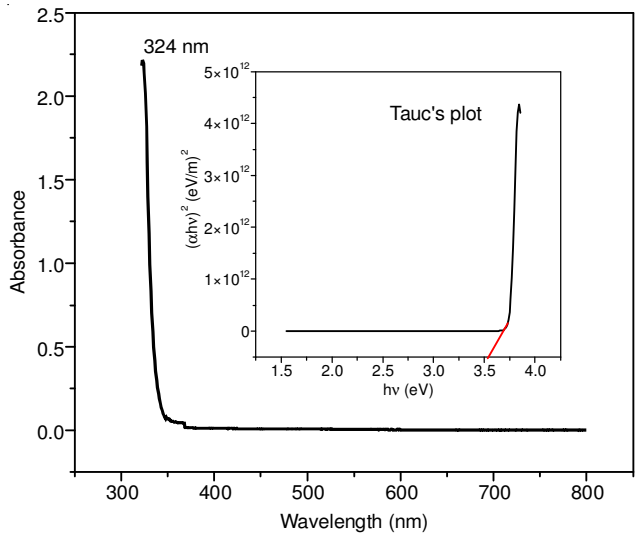

Fig. 6. Optical Absorption spectrum of LL5SS single crystal along with its Tauc plot (as inset)

Photoluminescence properties: The photoluminescence technique is the accurate method for determining the optical quality as well as its excitation fine structure [17]. The photoluminescence spectrum was recorded using a Perkin Elmer photoluminescence unit at room temperature with slit width 10 nm in the range of 350-650 nm. The LL5SS was excited at 324 nm and the emission spectrum was obtained as shown in Fig. 7. The strong luminescence broad peak at 432 nm was observed and is due to intermolecular interactions of lattice vibrations and indicates that the grown crystal has a violet fluorescence emission. This property of having strong emission in this range may lead to potential application of this material in optoelectronic devices [18]. The materials with photoluminescence of violet and deep red are found to be more useful for OLED applications and optical data storage applications [19]. Hence the broad luminescence profile gives information about the electronic property of the grown crystal.

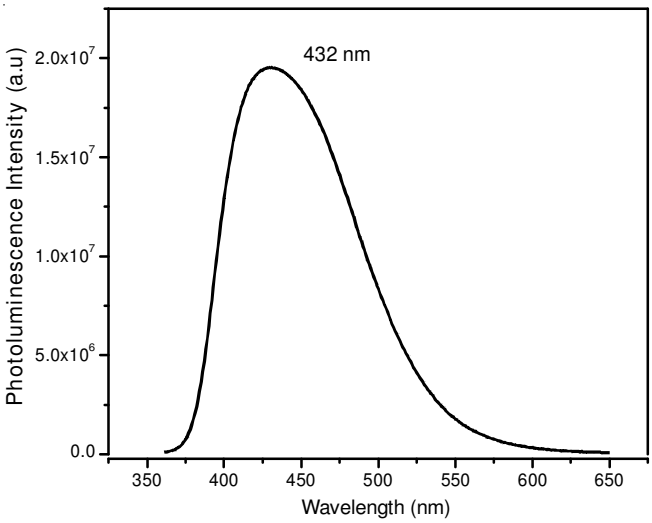

Fig. 7. Photoluminescence spectrum of the LL5SS crystal excited at 432 nm

Thermal analysis: Thermogravimetric analysis and differential thermal analysis gives information about the phase transition and various stages of decomposition of the crystal. Thermal analyses (TG/DTA) were performed by a Instrument: TGA Q500 V20.10 Build 36 and the spectrum is shown in Fig. 8. The three major exothermic peaks were observed at 118.4, 242.5 and 559.2 °C due to the major decomposition of material in the DTA curve. From the TG curve, it is observed that there was 7.8 % of weight loss around at 97.4 °C. This confirms the removal of water molecule in the sample. In the second stage of decomposition, sulfosalicylates, CO_2 and CH_4 get liberated with the weight loss of 65.87 % of the material [20]. Third stage of weight loss is due to the release of NH_3. Hence, the LL5SS material has reasonably good thermal stability which satisfies the requirement for the device fabrication.

Dielectric measurement: The dielectric measurements were carried out on the grown LL5SS single crystal with respect to the temperature and frequency. The well polished and good quality single crystal was subjected to dielectric measurements by using Numetriq PSM1735 equipped with resistive furnace and that is connected with a temperature controller (Eurotherm model No. 2404 with the accuracy of ± 1 °C). The dielectric

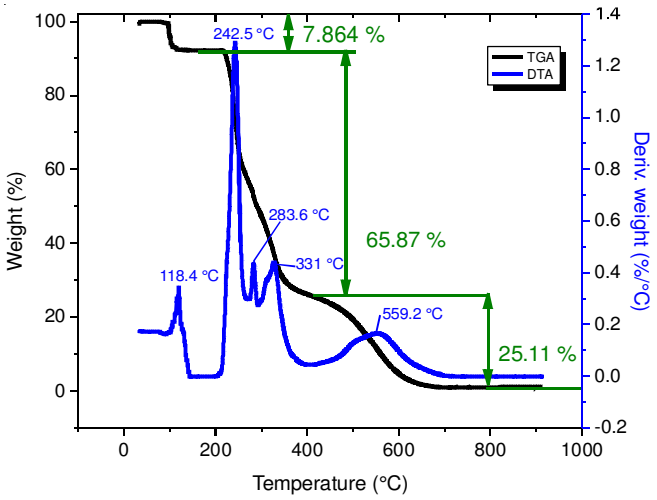

Fig. 8. TGA-DTA curve of LL5SS

constant ε_r indicates the ability of the dielectric to polarize and it can be defined as the ratio of the dielectric's permittivity to the permittivity of a vacuum:

$$\varepsilon_r = Ct/A\varepsilon_0$$

where A is the area of the plate, d is the distance between the two parallel plates. ε_0 is the absolute permittivity of the free space. The frequency dependence of the dielectric constant (ε) is shown in Fig. 9.

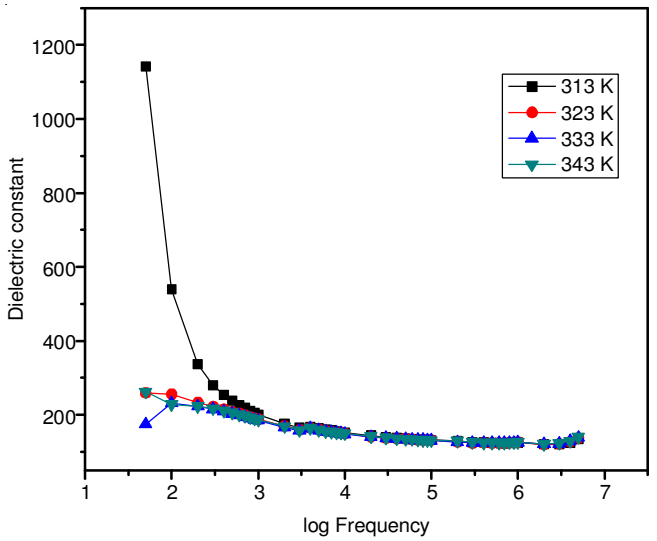

Fig. 9. Plot of log f *versus* dielectric constant for LL5SS crystal

The dielectric constant has high values in the lower frequency region and then it decreases with increasing the frequency. The high value of dielectric constant at low frequency may be due to the orientation, space charge, electronic and ionic polarization [21]. The increase in temperature leads to increase in dielectric constant and is due to the presence of electronic polarization. Dielectric loss is the absorption of energy by movement of charges in an alternating field and is particularly high around the relaxation and resonance frequencies of the polarization mechanisms. It is observed that the dielectric loss decreases with increasing frequency. The frequency dependence of the dielectric loss (ε) is shown in Fig. 10. The low dielectric loss at high frequencies indicates that the LL5SS possess enhanced optical quality with lesser defects and it is suitable for NLO application.

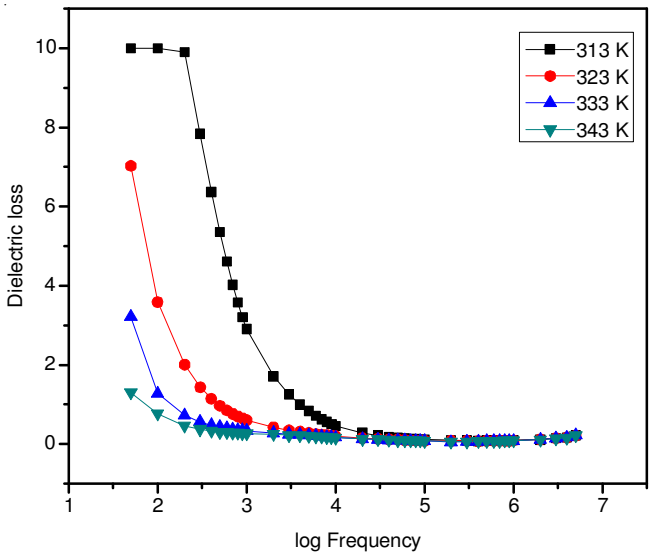

Fig. 10. Plot of log f *versus* dielectric loss for LL5SS crystal

Non-linear optical (NLO) studies

Second-order non-linear optical property: A high intensity Nd:YAG laser (λ = 1064 nm) with a pulse duration of 6 ns was passed through the powdered sample. The second harmonic signal produced in LL5SS was verified from the green light (λ = 532 nm) emission from the crystal. It is observed that the SHG efficiency of the grown single crystal is 0.87 times that of the standard KDP crystal

Third order non-linear optical property: Z-scan approach is a standard method for the precise assessment of intensity dependent non-linear refractive index n_2, non-linear absorption coefficient β and non-linear susceptibilities. OBIS CW laser of wavelength of 640 nm was used in this experiment. In the Z-scan technique a stepper motor was used to move a crystal sample across the +Z to -Z axial direction and thus the crystal sample will experience different light intensity at its various positions. The transmission of the beam through an aperture placed in the far field is measured using a photo detector fed to the digital power meter. Using the collected data of Z-scan, the difference between the normalized valley and peak transmittance ΔTp-v can be calculated by

$$\Delta T_{P-V} = 0.46(1-S)^{0.25}\left|\Delta\Phi\right| \quad (1)$$

where $|\Delta\Phi|$ is on axis phase shift at the focus, S is the aperture linear transmittance and it can be calculated by

$$S = 1 - \exp\left(\frac{-2r_a^2}{\omega_a^2}\right) \quad (2)$$

where r_a is the radius of the aperture and ω_a is the beam radius at the aperture.

L_{eff} is the effective thickness of the sample measured from

$$L_{eff} = \frac{[1-\exp(-\alpha L)]}{\propto} \quad (3)$$

where L is the thickness of the sample and a is the linear absorption coefficient. The value of non-linear refractive index (n_2) can be measured using the relation:

$$n_2 = \frac{\Delta\Phi}{KI_0L_{eff}} \quad (4)$$

where K is the wavenumber ($2\pi/\lambda$). The real parts of the third order non-linear susceptibility [χ^3] is determined by non-linear refractive index n_2 collected from the closed aperture Z-scan data employing the relation:

$$Re\chi^{(3)} = \frac{10^{-4}(\varepsilon_0 C^2 n_0^2 n_2)}{\pi}\left(\frac{cm^2}{W}\right) \quad (5)$$

The value the non-linear absorption coefficient β can be estimated from open aperture curve using the expression:

$$\beta = \frac{2\sqrt{2}\Delta T}{I_0 L_{eff}} \quad (6)$$

The imaginary parts of the third order non-linear susceptibility [χ^3] is determined by the non-linear absorption coefficient β employing the relation:

$$Im\chi^{(3)} = \frac{10^{-2}(\varepsilon_0 C^2 n_0^2 \lambda\beta)}{4\pi}\left(\frac{cm}{W}\right) \quad (7)$$

The third-order non-linear optical susceptibility is thus obtained by:

$$\chi^3 = \sqrt{Re(\chi^3)^2 + Im(\chi^3)^2} \quad (8)$$

Fig. 11 shows the normalized transmittance for the open aperture (OA) curve of LL5SS and the transmission is minimum at the focal point This indicates that the materials exhibit two-photon absorption (TPA).

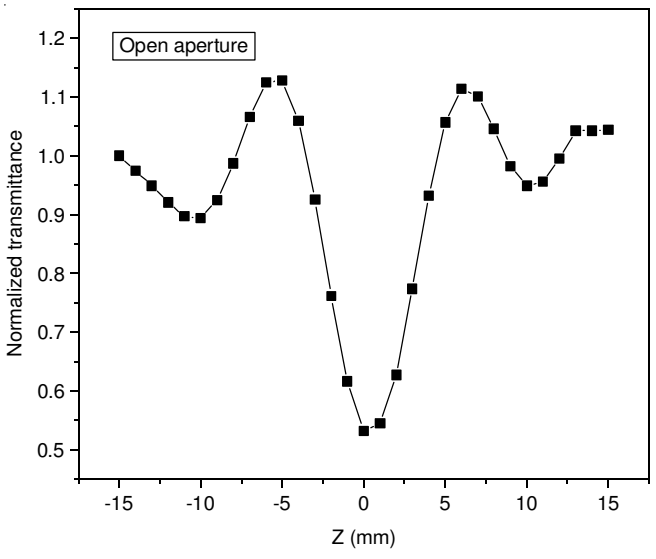

Fig. 11. Z-scan curve of LL5SS in open aperture

Fig. 12 shows the normalized transmittance for the closed aperture curve of LL5SS. The valley to peak configuration of the curve shows that the refractive index changes is positive, exhibiting a self-focusing effect. From the closed aperture curve, the pre-focal transmittance valley is followed by the post focal peak which is the signature of positive non-linearity

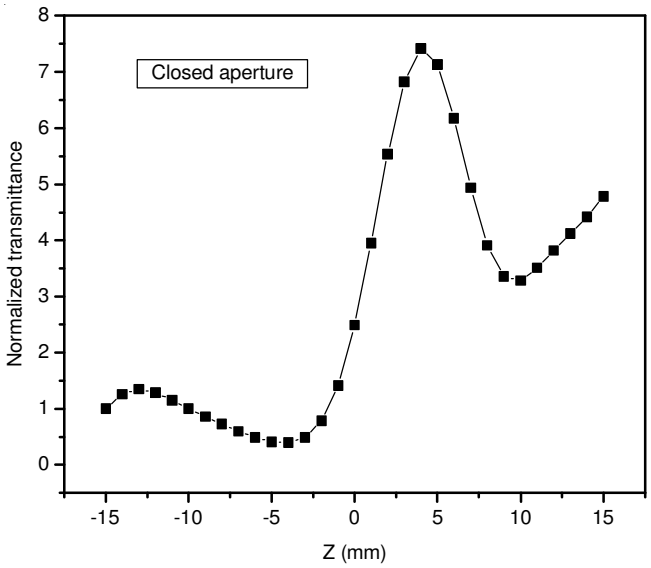

Fig. 12. Z-scan curve of LL5SS in closed aperture

[22] The large molecular polarizability of the material is responsible for high value of $\chi^{(3)}$ in the LL5SS crystal and is attributed to the π electron cloud movement from donor to acceptor levels [23,24].

This may be an advantage for the application in protection of optical sensors. Some of the third order non-linear parameters are tabulated in the Table-5.

TABLE-5
THIRD ORDER NON-LINEAR OPTICAL PARAMETER OF LL5SS

Laser beam wavelength (λ) (nm)	640
Lens focal length (f) (cm)	30
Optical path distance (Z) (cm)	85
Spot-size diameter in front of aperture (ω_a) (cm)	3.3
Aperture radius (ra) (mm)	2
Effective thickness (L_{eff}) (mm)	5.208×10^{-2}
Non-linear refractive index (n_2) (cm^2/W)	1.433×10^{-12}
Non-linear absorption coefficient (β) (cm/W)	2.4215×10^{-6}
Absolute susceptibility $\lvert\chi^{(3)}\rvert$ esu	5.326172×10^{-10}

Micro hardness studies: Hardness measures the resistance of a sample to material deformation due to a constant compression load from a object and extremely important as far as the fabrication of devices is concerned. The high quality of the polishing material significantly improves the hardness values [25]. The hardness number (H_V) is determined by the load over the surface area of the indentation and not the area normal to the force and is therefore not pressure. The hardness number of the grown crystal is calculated by using the following expression:

$$H_V = 1.8554\left(\frac{P}{d^2}\right)\ (kg/mm^2) \quad (9)$$

where P is the applied load in kg, d is the average length of indented impressions in mm and 1.8544 is a constant of geometrical factor for the diamond pyramidal indenter. The plot of H_V *versus* P is shown in the Fig. 13. From the plot, the hardness number increases with the applied load and that satisfies the reverse indentation size effect (RISE). The plot log (P) *versus* log (d) is shown in Fig. 14 and using this plot

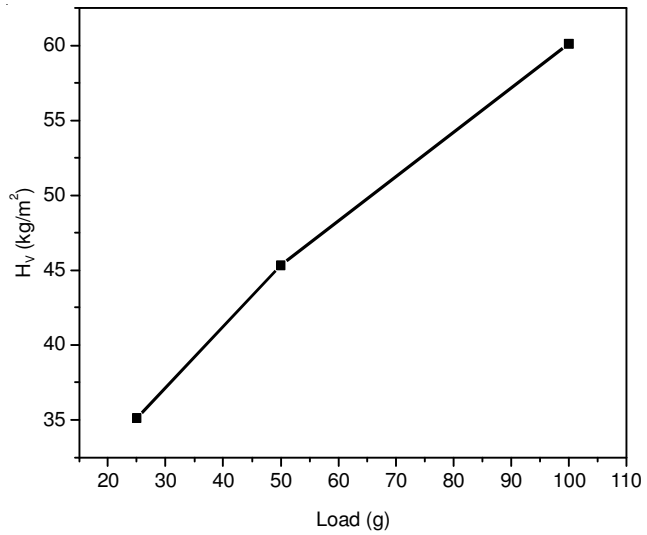

Fig. 13. Dependence of microhardness (H_v) on applied indentation load P of LL5SS crystal

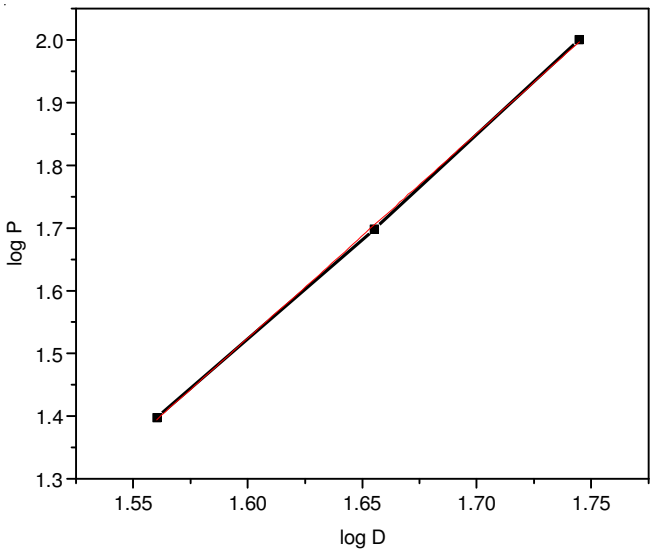

Fig. 14. Plot of log D *versus* log P of LL5SS crystal

the value of work hardening coefficient n was estimated. The n value was 3.26 which confirm that LL5SS crystal belongs to the soft material category. The elastic stiffness constant (C_{11}) for different loads (Fig. 15) calculated using Wooster's empirical formula:

$$C_{11} = H_v^{7/4} \quad (10)$$

The calculation of stiffness constant shows that the binding forces between the ions are strong.

The resistance to fracture indicates the toughness of a material K_c and is given by a relation:

$$K_C = \frac{P}{\beta_0 l^{3/2}}, l \geq \frac{d}{2} \quad (11)$$

where β_0 is the indenter constant, equal to 7 for the Vicker's diamond pyramid indenter.

Brittleness affects the mechanical behaviour of a material and gives information about the fracture induced in a material. Brittleness index (B_i) is calculated using relation:

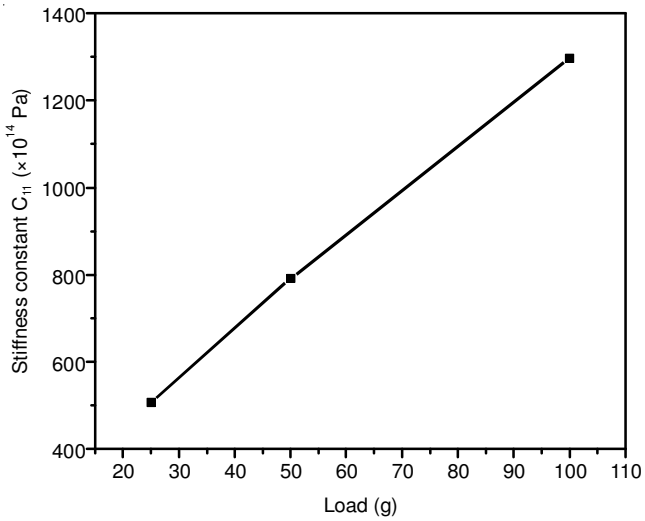

Fig. 15. Plot of load P *versus* stiffness constant of LL5SS crystal

$$\text{Brittleness index } (B_i) = \frac{H_V}{K_C} \quad (12)$$

The value hardness number (H_V), Stiffness constant (C_{11}) and Brittleness index (B_i) of LLSS was shown in the Table-6.

TABLE-6
MECHANICAL PARAMETERS OF LL5SS CRYSTAL

Load P (g)	Hardness number (H_V) (kg/mm^2)	Stiffness constant (C_{11}) ($\times 10^{14}$ Pa)	Toughness (K_c) g (μm)$^{3/2}$	Brittleness index (B_i) (μm)$^{3/2}$
25	35.11503	506.5390	1.755865	19.99871
50	45.32317	791.6996	3.511729	12.90622
100	60.10540	1297.474	7.023458	8.557807

Laser damage threshold (LDT) measurement: One of the important criteria for a NLO crystal to progress as a photonic device is its resistance to laser damage, since high optical intensities are involved in non-linear processes. The laser induced breakdown in the crystals caused by various physical processes such as multi photon absorption and electron avalanche for the transparent materials. A fundamental wavelength of 1064 nm Gaussian beam of pulse width 6 ns with a repetition rate of 10 Hz and was used to measure the laser damage threshold of LL5SS crystal. Laser damage threshold of the crystal was estimated using the relation:

$$\text{Power density } (P_d) = \frac{E}{\tau A} \quad (13)$$

where $A = \pi r^2$, E is the input energy (mJ), τ is the pulse width (ns) and r is the radius of the spot (mm). The calculated values of the LDT of 5.6 GW/cm^2. Good value of LDT indicates that a grown crystal contains a low defect and it can be used for device fabrication.

Conclusion

Single crystals of LL5SS were grown in aqueous solution using slow evaporation method. Single crystal X-ray analysis confirms that the crystals belong to the monoclinic system with space group $P2_1$. The various functional groups were confirmed by FTIR analysis. Optical assessment showed that it has UV-Visible absorption cut off at around 324 nm the

optical band gap energy is 3.536 eV calculated by Tauc's Plot. The photoluminescence of LL5SS single crystal has maximum intensity at 432 nm, which corresponds to violet emission. Dielectric studies show that the sample has low loss factor. Thermo gravimetric analysis showed the different decomposition stages. The SHG of LL5SS was confirmed by green light emission. The non-linear refractive index, absorption coefficient and third order susceptibility were found to be 1.433×10^{-12} cm^2/W, 2.4215×10^{-6} cm/W and 5.326172×10^{-10} esu, respectively. Vickers micro hardness test showed that the grown crystal belongs to soft material category. The laser damage threshold power density for the grown crystal is 5.6 GW cm^{-2}. All these studies indicates that the grown crystal possess good optical as well as mechanical properties towards the materials suitability for optical device fabrications.

Supplementary: CCDC: 1562492 contains the supplementary crystallographic data for the compound reported in this Article.

ACKNOWLEDGEMENTS

One of the authors (D. Jayalakshmi) is grateful to University Grants Commission, New Delhi, India for the support under minor research project scheme (No. F: MRP-5576/15(SERO/UGC) dated January 2015).

REFERENCES

1. J. Zyss, Molecular Non-Linear Optics, Academic Press, Boston (1994).
2. D.R. Yuan, D. Xu, N. Zhang, M.G. Liu and M.H. Jiang, *Chin. Phys. Lett.*, **13**, 841 (1996); https://doi.org/10.1088/0256-307X/13/11/011.
3. I. Ledoux, *Synth. Met.*, **54**, 123 (1993); https://doi.org/10.1016/0379-6779(93)91051-3.
4. H.A. Petrosyan, H.A. Karapetyan, M.Y. Antipin and A.M. Petrosyan, *J. Cryst. Growth*, **275**, 1919 (2005); https://doi.org/10.1016/j.jcrysgro.2004.11.258.
5. H.O. Marcy, L.A. DeLoach, J.-H. Liao, M.G. Kanatzidis, S.P. Velsko, M.J. Rosker, L.F. Warren, C.A. Ebbers, P.H. Cunningham and C.A. Thomas, *Opt. Lett.*, **20**, 252 (1995); https://doi.org/10.1364/OL.20.000252.
6. S.R. Marder, J.E. Sohn and G.D. Stucky, Materials for Non-linear Optics, ACS Symposium Series, p. 455 (1991).
7. S.S. Gupte, A. Marcano O, R.D. Pradhan, C.F. Desai and N. Melikechi, *J. Appl. Phys.*, **89**, 4939 (2001); https://doi.org/10.1063/1.1358325.
8. D. Arthi, E. Ilango, M. Mercina, D. Jayaraman and V. Joseph, *J. Mol. Struct.*, **1127**, 156 (2017); https://doi.org/10.1016/j.molstruc.2016.07.030.
9. K. Ramya, N.T. Saraswathi and C.R. Raja, *Opt. Laser Technol.*, **90**, 222 (2017); https://doi.org/10.1016/j.optlastec.2016.12.002.
10. N. Rani, N. Vijayan, K. Thukral, K.K. Maurya, G. Bhagavannarayana, D. Haranath, S. Verma and M.A. Wahab, *Spectrochim. Acta A Mol. Biomol. Spectrosc.*, **105**, 192 (2013); https://doi.org/10.1016/j.saa.2012.12.030.
11. V.S. Shankar, R. Sankar, R. Siddheswaran, R. Jayavel and P. Murugakoothan, *Mater. Chem. Phys.*, **109**, 119 (2008); https://doi.org/10.1016/j.matchemphys.2007.11.008.
12. J.-F. Ma, J. Yang, Li, S.-Y. Song, H.-J. Zhang, H.-S. Wang and K.-Y. Yang, *Cryst. Growth Des.*, **5**, 807 (2005); https://doi.org/10.1021/cg049723a.
13. A. Cote and G.K.H. Shimizu, *Coord. Chem. Rev.*, **245**, 49 (2003); https://doi.org/10.1016/S0010-8545(03)00033-X.
14. O.M. Yaghi, C.E. Davis, G. Li and H. Li, *J. Am. Chem. Soc.*, **119**, 2861 (1997); https://doi.org/10.1021/ja9639473.
15. C. Swiegers and T. Malefetse, *Chem. Rev.*, **100**, 3483 (2000); https://doi.org/10.1021/cr990110s.
16. S.A.M.B. Dhas and S. Natarajan, *Cryst. Res. Technol.*, **43**, 869 (2008); https://doi.org/10.1002/crat.200711152.
17. L. Kumari and W.Z. Li, *Cryst. Res. Technol.*, **45**, 311 (2010); https://doi.org/10.1002/crat.200900600.
18. M. Jose, R. Uthrakumar, A.J. Rajendran and S.J. Das, *Spectrochim. Acta Part A: Mol. Biomol. Spectrosc.*, **86**, 495 (2012); https://doi.org/10.1016/j.saa.2011.11.002.
19. A. Aravindan, P. Srinivasan, N. Vijayan, R.G. Krishnan and P. Ramasamy, *Spectrochim. Acta Part A: Mol. Biomol. Spectrosc.*, **71**, 297 (2008); https://doi.org/10.1016/j.saa.2007.12.023.
20. M. Roman and W.T. Winter, Biomacromolecules, 5, 1671 (2004); https://doi.org/10.1021/bm034519+.
21. R.R. Babu, K. Sethuraman, N. Vijayan, G. Bhagavannarayana, R. Gopalakrishnan and P. Ramasamy, *Cryst. Res. Technol.*, **41**, 906 (2006); https://doi.org/10.1002/crat.200510693.
22. T.H. Wei, D.J. Hagan, M.J. Sence, E.W. Van Stryland, J.W. Perry and D.R. Coulter, *Appl. Phys. B*, **54**, 46 (1992); https://doi.org/10.1007/BF00331733.
23. A.J. Kiran, D. Udayakumar, K. Chandrasekharan, A.V. Adhikari and H.D. Shashikala, *J. Phys. At. Mol. Opt. Phys.*, **39**, 3747 (2006); https://doi.org/10.1088/0953-4075/39/18/005.
24. C. He, Y. Wu, G. Shi, W. Duan, W. Song and Y. Song, *Org. Electron.*, **8**, 198 (2007); https://doi.org/10.1016/j.orgel.2007.01.002.
25. N. Sivakumar and G. Anbalagan, *Opt. Mater.*, **60**, 533 (2016); https://doi.org/10.1016/j.optmat.2016.09.010.